UNIVERSITY OF BATH

University of Bath

Alternative formats
If you require this document in an alternative format, please contact:
openaccess@bath.ac.uk

Manuscript Details

Manuscript number	OLEN_2019_530_R1
Title	Enhanced 6D Measurement by Integrating an Inertial Measurement Unit (IMU) with a 6D Sensor Unit of a Laser Tracker
Article type	Full Length Article

Abstract

Six-degree-of-freedom (6D) sensors enhance the measurement capability of traditional three-degree-of-freedom (3D) laser trackers. However, the classical 6D measurement techniques still have shortcomings in actual use, such as the problem of line of sight and relatively low data acquisition rate. The proposed approach by integrating an Inertial Measurement Unit (IMU) with a 6D sensor unit of a laser tracker is effective to overcome these limitations. The error is corrected by the combination of Kalman filter and a backward smoothing algorithm. The Kalman filter only works when the 6D sensor's data coms, while the backward smoothing algorithm works during the whole process. The experiments are performed to compare the error in three positions and three rotational orientations between the proposed method and the Kalman filter and evaluate the effects of different rates and IMU frequencies on the algorithm. The simulations are also performed to estimate the maximum outage time. The results verify that the proposed method can solve the problem of line of sight and low data acquisition rate effectively.

Keywords	laser tracker, 6D sensor, 6D measurement, IMU, data fusion, optical dimensional metrology
Taxonomy	Laser Beam Delivery, Time Domain Processing
Corresponding Author	Jiarui Lin
Order of Authors	Linghui Yang, Ruiying Liao, Jiarui Lin, Bo Sun, Zheng Wang, Patrick Keogh, Jigui Zhu
Suggested reviewers	Richard Leach, Weihu Zhou, Kechen Song, Xiaoli Liu

Submission Files Included in this PDF

File Name [File Type]

cover letter.docx [Cover Letter]

Response.docx [Response to Reviewers]

Highlights.docx [Highlights]

Manuscript.docx [Manuscript File]

Figure1.docx [Figure]

Figure2.docx [Figure]

Figure3.docx [Figure]

Figure4.docx [Figure]

Figure5.docx [Figure]

Figure6.docx [Figure]

Figure7.docx [Figure]

Figure8.docx [Figure]

Figure9.docx [Figure]

Figure10.docx [Figure]

Table1.docx [Table]

Table2.docx [Table]

Table3.docx [Table]

Conflict of interest statement.docx [Conflict of Interest]

To view all the submission files, including those not included in the PDF, click on the manuscript title on your EVISE Homepage, then click 'Download zip file'.

Research Data Related to this Submission

There are no linked research data sets for this submission. The following reason is given:
The data that has been used is confidential

Corresponding Author:

Jiarui Lin

Associate Professor

State Key Laboratory of Precision Measuring Technology and Instruments

Tianjin, China, 300072

linjr@tju.edu.cn

+86 13602063885

Dear editor,

Here within enclosed is our paper for consideration to be published in **"Optics and Lasers in Engineering"**. Further information about the paper is in the following:

The Title: Enhanced 6D Measurement by Integrating an Inertial Measurement Unit (IMU) with a 6D Sensor Unit of a Laser Tracker

The Authors: Linghui Yang, Ruiying Liao, Jiarui Lin, Bo Sun, Zheng Wang, Patrick Keogh, Jigui Zhu

No conflict of interest exists in the submission of this manuscript, and the manuscript is approved by all authors for publication. The authors claim that the work described is original research that has not been published previously, and not under consideration for publication elsewhere, in whole or in part. All the authors listed have approved the manuscript that is enclosed.

Six-degree-of-freedom (6D) sensors increase greatly the measurement capability of traditional three-degree-of-freedom (3D) laser trackers. However, there are two main limitations in current 6D sensors. The basic limitation is the requirement of a clear line of sight between the tracker and sensor. The data are irretrievable during the outage periods. The second limitation is that the data acquisition rates of 6D sensors are limit by zoom camera of a laser tracker, which is typically only 100Hz. To overcome these limitations, an enhanced 6D measurement method by integrating an Inertial Measurement Unit (IMU) with a 6D sensor unit of a laser tracker is proposed. Measurements from the IMU and the 6D sensor unit are fused using a Kalman filter and a backward smoothing algorithm. The experimental results show that the proposed data fusion method is more stable than using a classical Kalman filter only. When the frequency of IMU was 2000 Hz, the raw laser tracking data were 2 Hz, the RMS errors of Kalman filter in X positions was 1.182 mm. While the RMS errors of the proposed method are 0.031 mm. Other conclusions can be drawn that low speed guarantees high precision, and the frequency of the IMU is high enough that it does not affect measurement accuracy in practical applications. According to the simulations, the proposed method supports an outage period of the laser tracker within 3 seconds.

I hope this paper is suitable for **"Optics and Lasers in Engineering"**. We deeply appreciate your consideration of our manuscript, and we look forward to receiving comments from the reviewers.

Sincerely,

Jiarui Lin

Dear Editors and Reviewers:

Thank you for your efforts and comments concerning our manuscript entitled "Enhanced 6D Measurement by Integrating an Inertial Measurement Unit (IMU) with a 6D Sensor Unit of a Laser Tracker "(ID: OLEN _2019_530). Those comments are helpful for improving our paper. We revised the manuscript in accordance with the reviewers' comments. The revised contents are colored in red. To be honest, with the help of the reviewers' comments, we think the paper has been improved a lot. We appreciate the comments very much.

Here below is our description on revision according to the reviewers' comments.

---List of Responses---

Reviewer #1:
1. Response to comment:

In the abstract, the description and conclusion of the method should be more detailed.

The authors' response:

This paper mainly solves the problem about the line of sight and low data acquisition rate in the 6D sensor unit of a laser tracker. To overcome these limitations, a system integrated by the inertial measurement unit (IMU) and the 6D sensor unit is proposed. The IMU has a high data rate and is completely self-contained. Therefore, sensor fusion can achieve greater advantages.

Measurements from the IMU and the 6D sensor unit are fused using a Kalman filter and a backward smoothing algorithm. Kalman filter is a conventional algorithm for data fusion. However, merely using a Kalman filter cannot match the accuracy of the laser tracker. Since the Kalman filter can only correct the error when acquiring the 6D sensor's data. The backward smoothing algorithm can correct the data between time t_{IMU} (Fig.2 (b)). Theoretically, the backward smoothing algorithm is more accurate than a Kalman filter. With our experiments, the following comments are obtained:

1. The proposed method is more stable and accurate than a classical Kalman filter. For example, when the frequency of IMU was 2000 Hz, the raw laser tracking data were 2 Hz, the RMS errors of Kalman filter in X positions was 1.182 mm. While the RMS errors of the proposed method are 0.031 mm.
2. The low speed guarantees high precision in our method. And the frequency of the IMU is too high to affect measurement accuracy.
3. The proposed method can solve the problem as previously mentioned. According to the simulations, the proposed algorithm supports an outage within 3 seconds.

Revise content: Abstract.

Considering the Reviewer's suggestion, we make a more detailed description and conclusion of our method. The abstract is modified.

2. Response to comment:

The symbol ( )$_X$ in Eq.3 should be explained.

The authors' response:

The symbol $( )_\times$ represents antisymmetric matrix. For example,

$$\omega = \begin{bmatrix} \omega_x & \omega_y & \omega_z \end{bmatrix}^T$$

$$(\omega)_\times = \begin{bmatrix} 0 & -\omega_z & \omega_y \\ \omega_z & 0 & -\omega_x \\ -\omega_y & \omega_x & 0 \end{bmatrix}$$

Revise content: Section 3.1.1

According to the Reviewer's suggestion, we have explained the symbol $( )_\times$.

3. Response to comment:

In Figure 3, "probing points" should change to "probing tip".

The authors' response:

It is a clerical error. The "probing points" should be changed to "probing tip".

Revise content: Section 3, Fig 3

The "probing points" have been changed to "probing tip".

4. Response to comment:

In Sec 3.2, explain why the backward smoothing algorithm is better than the Kalman filter.

The authors' response:

In Fig.2 (b), the blue line is the integral process of IMU. Since the data of the 6D sensor occur at time $_{tracker(+)}$, the accumulated error eliminate suddenly. But the error during the t_{IMU} still exist. The backward smoothing algorithm starts with time $t_{tracker(+)}$ and reverses filtering fusion of data. The error is shown in the red line. Therefore, the backward smoothing algorithm is more accurate than the Kalman filter theoretically.

Revise content: Senction 3.2

Thank you for your kindly suggestion. We have explained it in Section 3.2.

Reviewer #2:

Thanks for reading.

Other changes:

1. Section 1, we have adjusted our introduction. Especially in paragraph 5, we emphasized the benefit of our method. Our enhanced 6D system mainly solve the limitation of line of sight and low data rate problem under the premise of ensuring accuracy.
2. Section 3, we have adjusted the description order in paragraph 1. First we

introduced the calibration between IMU and 6D sensor in brief, and then illustrated the characteristics of the Kalman filter and backward smoothing.

3. Section 4, we added the description of aims of experiments in each subsection.
4. Section 4.1, the comparation results between the Kalman filter and our method are described more concisely.
5. Fig. 6, the explaination of curve were added.
6. Section 4.2, "the frequencies of the T-Mac were set to seven values" was changed to "the frequencies of T-Mac were set to 100 Hz, 50 Hz, 20 Hz, 10 Hz, 5 Hz, 2 Hz, and 1 Hz".
7. Section 4.3, the conclusion part was changed to "From Fig.9, as the frequency of IMU increases, the errors of 6D in both Kalman filter and our smoother method are not regular. The reason is the frequency of IMU is high enough to make results irregular. It can be inferred that as the data rate is high enough, the frequency of IMU is not the main factor to affect data fusion accuracy."
8. Section 4.4, "The references correspond to 90 seconds of measurement time." was changed to "The simulation time is 90 seconds." And the text layout of this part has also been adjusted.
9. Acknowledgements, the acknowledgements have been updated.
10. Reference, the reference have been updated.
11. Section 5, the conclusion part has been slight modified to make the language more fluent.

Thank all reviewers for their comments and useful suggestions.

We have tried our best to improve the manuscript and made changes in the manuscript. We appreciate for Editors/Reviewers' efforts and hope that the revision will meet with approval.

Sincerely,
Jiarui Lin
(E-mail: linjr@tju.edu.cn)

Highlights

• The acquisition rate of 6D Sensor Unit of a laser tracker is increased and the problem of line of sight is solved by integrating an IMU.

• A Kalman filter and a backward smoothing algorithm is fusing to ensure high precision in 6D including three positions and three rotational orientations.

• The accuracy of proposed algorithm, the influence of T-mac frequency and system velocity are verified by a series of comparative experiments.

• The maximum outage time is determined by simulations.

Enhanced 6D Measurement by Integrating an Inertial Measurement Unit (IMU) with a 6D Sensor Unit of a Laser Tracker

Linghui Yang[1], Ruiying Liao[1], Jiarui Lin[1, *], Bo Sun[1], Zheng Wang[2], Patrick Keogh[2] and Jigui Zhu[1]

[1] *State Key Laboratory of Precision Measuring Technology and Instruments, Tianjin University, Tianjin, China*

[2] *Department of Mechanical Engineering, University of Bath, Bath BA2 7AY, United Kingdom*

Abstract

Six-degree-of-freedom (6D) sensors enhance the measurement capability of traditional three-degree-of-freedom (3D) laser trackers. However, the classical 6D measurement techniques still have shortcomings in actual use, such as the problem of line of sight and relatively low data acquisition rate. The proposed approach by integrating an Inertial Measurement Unit (IMU) with a 6D sensor unit of a laser tracker is effective to overcome these limitations. The error is corrected by the combination of Kalman filter and a backward smoothing algorithm. The Kalman filter only works when the 6D sensor's data coms, while the backward smoothing algorithm works during the whole process. The experiments are performed to compare the error in three positions and three rotational orientations between the proposed method and the Kalman filter and evaluate the effects of different rates and IMU frequencies on the algorithm. The simulations are also performed to estimate the maximum outage time. The results verify that the proposed method can solve the problem of line of sight and low data acquisition rate effectively.

Keywords: laser tracker, 6D sensor, 6D measurement, IMU, data fusion, optical dimensional metrology

1. Introduction

Six-degree-of-freedom (6D) measurement systems have been investigated widely

---

* Corresponding author
Email address: linjr@tju.edu.cn

in applications such as navigation and detection [1, 2], motion tracking [3-5] and three-degree-of-freedom (3D) measurement [6, 7]. Measurement systems based on 6D sensors of a laser tracking can fulfill requirement in most measurement tasks [8, 9]. Laser trackers have characteristics of high accuracy, reliability, durability, mobility, large working volume (up to hundred meters), flexible layout, and a high degree of automation. In addition to single-point reflector measurement, the 6D laser tracking system that acquire not only position (x, y, and z) but also rotational orientation (roll, pitch, and yaw) data, which expands the measurement scope and the applications of traditional 3D laser trackers. In universal using process of 6D laser tracking system, the 6D sensors are attached to the measured object directly, and the laser tracker serves as the reference to acquire 6D information. Several 6D sensors have been proposed in prior literatures which mainly differ in their rotational orientation determination approaches. A classic one is reported in [10], where a cluster of LED targets surrounding the reflector with known geometry is captured by a separate motorized zoom camera. The rotational orientation is determined from a standard space resection. Another well-known method is introduced in [11]. A pinhole retro-reflector is used, where the apex of the prism is removed. Part of the tracker beam passes through the pinhole and projects onto an image sensor. The pitch and yaw angles are determined by a perspective projection, and the roll angle is determined by a tilt sensor. Other works about 6D sensors are presented in [12-16].

However, there are still limitations in current 6D sensors. The basic limitation is the requirement for a clear line of sight between the tracker and sensors. It is common to find that 6D data is lost in cases of the beam or LED cluster interruptions [10, 11], particularly in cluttered environments or when undertaking complex measurement tasks. Though the auto-lock algorithms have been developed to cope with beam interruption and the sophisticated omnidirectional sphere reflectors have been designed, the prudent operation is still need to avoid data loss. Sometimes, the viewing position of the tracker must be moved to measure hidden points, whose labor cost slow down the measurement process. For all these, the line of sight issue still cannot addressed completely because data are irretrievable during the outage periods.

A second limitation is that the data acquisition rate of the 6D sensors are limited by individual sensor performance, such as low shutter speed for an image sensor and low-frequency response for a tilt sensor. Taking the classic 6D laser tracking system for instance, the bandwidth is limited by the zoom camera of a laser tracker, which is typically only 100 Hz [26] (Figure 1). However, the low data rate cannot meet certain cases. For example, the 6D motion of a portable stereo line-scan sensor [7] require the data processing frequencies greater than a few kilohertz. Considering the trade-off between frame rate, resolution, and pixel size, it is difficult to increase the frame rate further. Additionally, as the data rate increases, it will be more difficult to recognize and distinguish the LED targets.

In order to overcome these limitations, this paper presents an enhanced 6D measurement approach by integrating an Inertial Measurement Unit (IMU) with a 6D sensor unit of a laser tracker. In the case of laser tracker outages that are caused by loss of line of sight between the 6D sensor unit and the laser tracker, the IMU is used instead

for 6D positioning. It is completely self-contained after power-up and may operate in any environment. Secondly, the integrated system is able to work at a superior data processing rate that coincides with the IMU's sampling rate. It has a considerably higher data rate (up to 10 kHz) when compared to that of laser trackers. These features will contribute to performance improvements for a 6D laser tracker, in terms of robustness, flexibility, and data rate.

Considering the cost and portability, a Micro-Electro-Mechanical System (MEMS) IMU was proposed in [17]. However, MEMS IMUs are typically very noisy and signals may drift. Due to the integral property, the accumulated error caused by drift increases rapidly over time. Therefore, the IMU is usually used with an aiding sensor to correct the error, such as GPS and vision sensors [18-21]. The Kalman filter and its derivatives are universally recognized in fusing IMU and other sensors' signals [22, 23]. And these integrate systems are widely used in simultaneous localization and mapping (SLAM) [24]. However, the accuracy of localization and the Kalman filter is too low to fulfill the measurement requirements. Therefore, in this paper, a Kalman filter is followed by a backward smoothing algorithm [25], and the 6D laser tracker behaves as an additional sensor to improve the overall performance. In this way, the integrated system can solve the limitation of line of sight and low data rate problem under the premise of ensuring accuracy.

The remaining of the paper is organized as follows: Section 2 describes the system configuration. Section 3 explains the basic theory of the proposed method, including the Kalman filter and backward smoothing algorithm. Experiments comparing the proposed method with classical Kalman filtering are reported in Section 4. Furthermore, the impact of various kinematic velocities, IMU and 6D laser tracker bandwidths on the algorithm are also analyzed. In addition, simulations are made to estimate the maximum allowable outage time. Finally, conclusions are summarized in Section 5.

2. System Description

The main hardware components that constitute the system are shown in Fig. 1. The system consists of a commercial 6D Laser Tracker System, which incorporates a laser tracker with a 6D sensor unit called T-Mac (AT 901 LR & T-Cam & T-Mac, Leica Geosystems) [26], and an IMU (STIM 300, Sensonor AS) composed of three gyro sensors and three accelerometers [27]. The IMU is attached rigidly to the T-Mac to constitute an integrated 6D sensor. The laser tracker measures location and angular attitude of the T-Mac whenever the retro-reflector and at least three LED markers are in sight. The IMU estimates triaxial angular rates and accelerations, from which position and attitude can be calculated by an integration algorithm. The two systems work with a common clock but with different data processing rates.
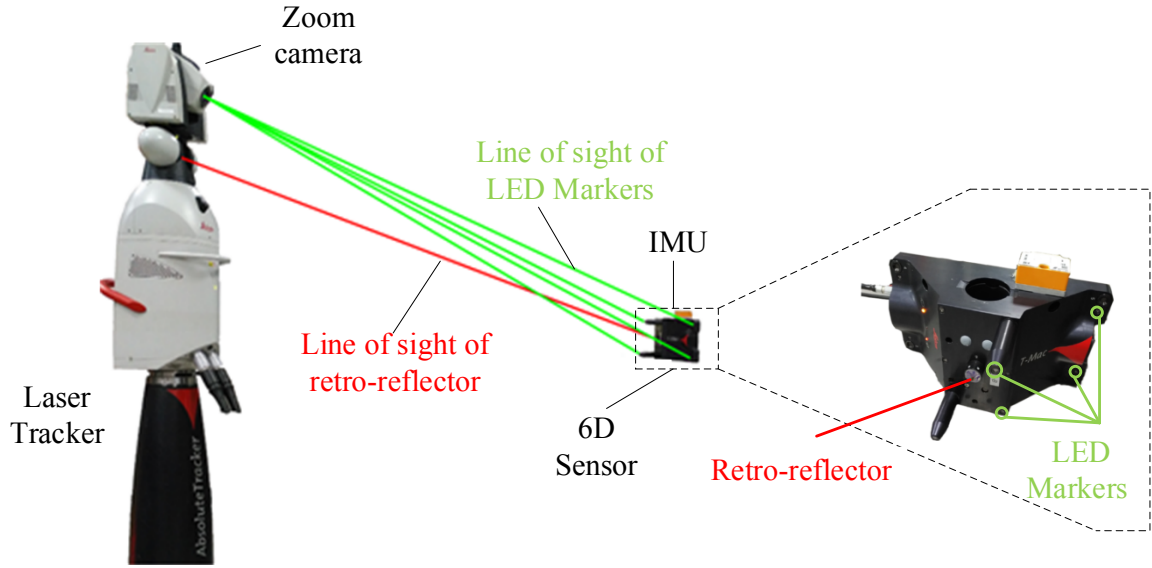
Figure 1. Configuration of the multi-sensor system.

The 6D laser tracker and IMU are heterogeneous systems. The general idea of the proposed method is that the IMU is used to bridge the laser tracker outages whereas the laser tracker is used for the in-motion correction of the IMU errors. The workflow is described in Fig. 2. Laser tracker outages stem from two major aspects, namely, the gaps between successive tracker measurements and loss of line of sight between the 6D sensor unit and the laser tracker. In the case of laser tracker outages, the IMU provides 6D positioning on its own until the tracker signal is recovered. This feature reduces the line of sight concerns and enables the sensor unit to move along its commanded measurement path, as long as the tracker can recapture the 6D sensor signals after an interruption. In our algorithm, data from two systems are fused and therefore a continuous and high-rate measurement can be accomplished regardless of momentary laser tracker outages.

In the case of outages, the position and attitude errors at none-tracker clock times are completely governed by the IMU errors as shown in Fig. 2(b). The accumulated errors increase with time until the end of the outage. To deal with these errors, a data fusion algorithm is applied each time a new laser tracker measurement arrives. At time $t_{tracker}(+)$, the accumulated errors of the IMU are estimated and corrected by fusing the data from both systems. As shown in Fig. 2(b), the errors can be corrected only at time $t_{tracker}(+)$ in classical Kalman filtering. With backward smoothing, the errors between times t_{IMU}... can also be corrected. This procedure is to be repeated throughout the entire measuring process.
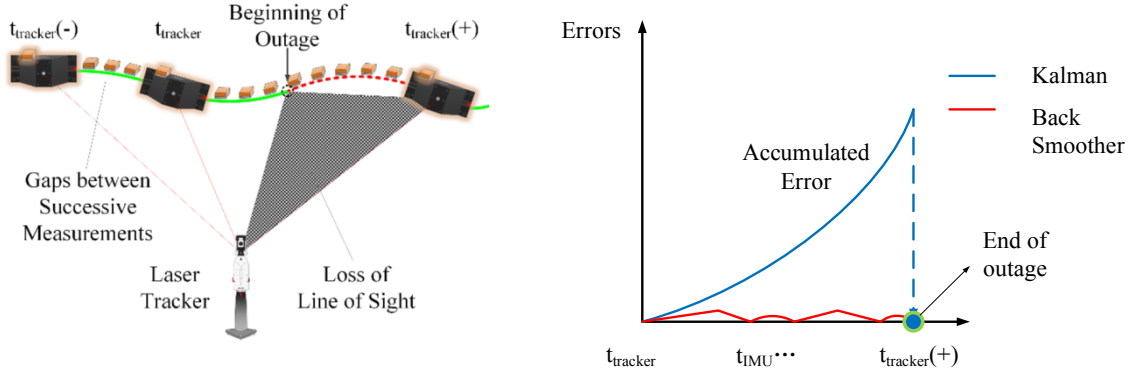
Figure 2. Diagram of the workflow and the error propagation. (a) The main workflow, (b) accumulated errors of the IMU during tracker outages.

3. Principle of the Proposed Method

The rigid transformations from IMU to 6D sensor is calibrated geometrically in advance. As depicted in Fig. 3(a), the IMU body frame (O_b-$X_b Y_b Z_b$) is defined with its origin at the lower-left corner, and the axes are perpendicular to the mechanical housing. The IMU body frame is constructed in the laser tracker frame by using a probing tip. In Fig. 3(b), the 6D sensor frame (O_s-$X_s Y_s Z_s$) and laser tracker (O_r-$X_r Y_r Z_r$) are also defined. The 6D transformation between the IMU and the 6D sensor unit is determined by taking the laser tracker as an intermediate frame. R_s^r and T_s^r are the rigid transformations from the 6D sensor frame to the laser tracker frame. R_b^r and T_b^r represent the rigid transformation from the IMU body frame to the laser tracker frame. The described method is relatively straightforward to implement and does not require compensation of IMU bias and noise errors, unlike existing approaches such as modified hand-eye calibration [28].

(a)   (b)
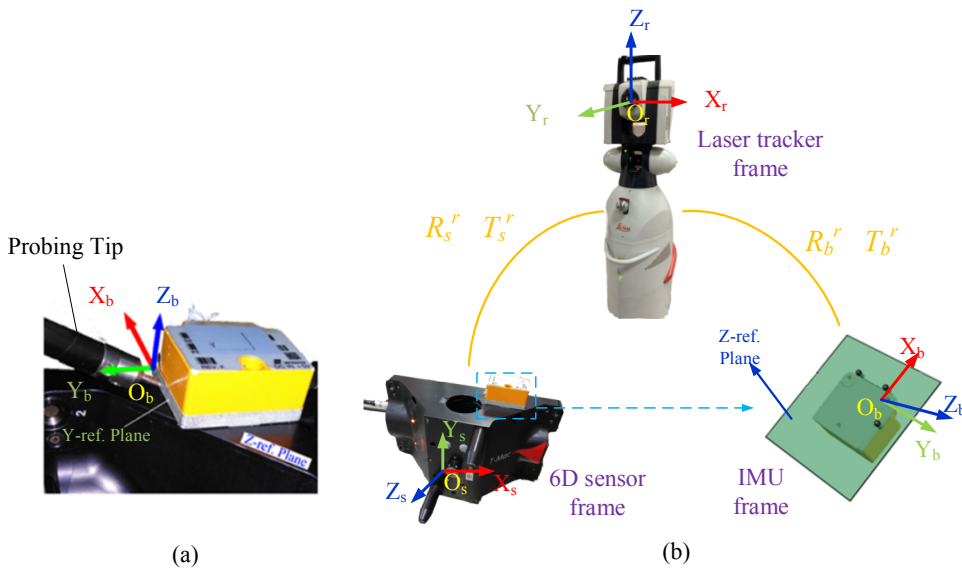
Figure 3. Calibration of the IMU-6D sensor unit relative pose. (a) Definition of the IMU body frame, (b) calibration by probing tip.

5

The emphases of this paper is to solve the accumulated error of the data during the outage time. It is dealt by two steps. First, the Kalman filter is used to correct the error at the tracker measurement time. It can remove most error at tracker measurement time. Second, the errors at IMU time are compensated by a backward smoothing algorithm. Throughout this paper, a symbol with an accent (^) represents an estimated variable, while the tilde accent (~) represents a noisy measurement. A subscript for a transformation represents the source frame, while the corresponding superscript represents the destination frame.

3.1 Kalman Filter

A closed-loop configuration of an error state is implemented, as depicted in Figure 4. The IMU serves to keep updating estimates according to its kinematics. When a full 6D measurement set is received, the Kalman filter will be executed, errors will be estimated and corrections injected into the nominal states. Then the corrected estimates are fed back and used as prior information for follow-on process.
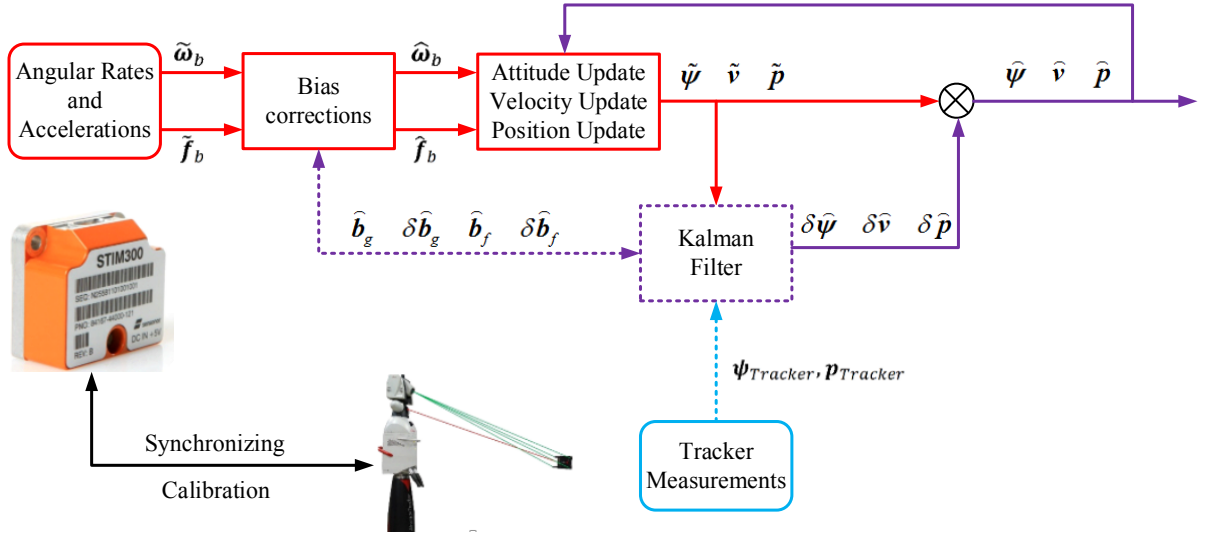
Figure 4. Block diagram of the integrated system incorporating a Kalman filter.

The Kalman filter estimates the attitude, velocity, and position errors. The attitude is described using the Euler angle representation. In order to facilitate accurate state estimates, the errors in the IMU signals, which are not directly measurable, are modeled and estimated. The static bias is modeled as a random constant process. The dynamic bias is modeled as a first-order Gauss-Markov process [29]. The error state is described by the vector

$$\delta \hat{\boldsymbol{x}} = \begin{bmatrix} \delta \hat{\boldsymbol{\psi}}^T & \delta \hat{\boldsymbol{v}}^T & \delta \hat{\boldsymbol{p}}^T & \boldsymbol{b}_g^T & \boldsymbol{b}_f^T & \delta \hat{\boldsymbol{b}}_g^T & \delta \hat{\boldsymbol{b}}_f^T \end{bmatrix}^T \tag{1}$$

Vectors $\delta \hat{\boldsymbol{\psi}}$, $\delta \hat{\boldsymbol{v}}$ and $\delta \hat{\boldsymbol{p}}$ are Euler angles, velocity, and position errors, respectively. Vectors $\hat{\boldsymbol{b}}_g$, $\hat{\boldsymbol{b}}_f$, $\delta \hat{b}_g$, and $\delta \hat{b}_f$ denote the static and dynamic biases of the gyroscopic and accelerometer measurements, respectively.

3.1.1 System Equations

The Kalman filter error state system model is given by

$$\delta \dot{\hat{\boldsymbol{x}}}(t) = \boldsymbol{F}(t)\delta \hat{\boldsymbol{x}}(t) + \boldsymbol{G}(t)\boldsymbol{\eta}(t) \tag{2}$$

The system matrix, $\boldsymbol{F}$, and noise covariance matrix, $\boldsymbol{G}$, are expressed in terms of 3×3 submatrices as follows:

$$\boldsymbol{F}(t) = \begin{bmatrix} \boldsymbol{0} & \boldsymbol{0} & \boldsymbol{0} & \hat{\boldsymbol{R}}_b^t & \boldsymbol{0} & \hat{\boldsymbol{R}}_b^t & \boldsymbol{0} \\ \left[\left(\hat{\boldsymbol{R}}_b^t (\tilde{\boldsymbol{f}}_b - \hat{\boldsymbol{b}}_f - \delta \hat{\boldsymbol{b}}_f) \right)_\times \right] & \boldsymbol{0} & 0 & \boldsymbol{0} & \hat{\boldsymbol{R}}_b^t & \boldsymbol{0} & \hat{\boldsymbol{R}}_b^t \\ \boldsymbol{0} & \boldsymbol{I} & \boldsymbol{0} & \boldsymbol{0} & \boldsymbol{0} & \boldsymbol{0} & \boldsymbol{0} \\ \boldsymbol{0} & \boldsymbol{0} & \boldsymbol{0} & \boldsymbol{0} & \boldsymbol{0} & \boldsymbol{0} & \boldsymbol{0} \\ \boldsymbol{0} & \boldsymbol{0} & \boldsymbol{0} & \boldsymbol{0} & \boldsymbol{0} & \boldsymbol{0} & \boldsymbol{0} \\ \boldsymbol{0} & \boldsymbol{0} & \boldsymbol{0} & \boldsymbol{0} & \boldsymbol{0} & diag[-\frac{1}{\tau_g}] & \boldsymbol{0} \\ \boldsymbol{0} & \boldsymbol{0} & \boldsymbol{0} & \boldsymbol{0} & \boldsymbol{0} & \boldsymbol{0} & diag[-\frac{1}{\tau_f}] \end{bmatrix} \tag{3}$$

$$\boldsymbol{G} = \begin{bmatrix} \hat{\boldsymbol{R}}_b^t & \boldsymbol{0} & \boldsymbol{0} & \boldsymbol{0} \\ \boldsymbol{0} & \hat{\boldsymbol{R}}_b^t & \boldsymbol{0} & \boldsymbol{0} \\ \boldsymbol{0} & \boldsymbol{0} & \boldsymbol{0} & \boldsymbol{0} \\ \boldsymbol{0} & \boldsymbol{0} & \boldsymbol{0} & \boldsymbol{0} \\ \boldsymbol{0} & \boldsymbol{0} & \boldsymbol{0} & \boldsymbol{0} \\ \boldsymbol{0} & \boldsymbol{0} & \boldsymbol{I} & \boldsymbol{0} \\ \boldsymbol{0} & \boldsymbol{0} & \boldsymbol{0} & \boldsymbol{I} \end{bmatrix}$$

These matrices are derived based on the IMU error kinematics in [30]. In Eq. (3), $\hat{\boldsymbol{R}}_b^t$ is the rotation matrix from the IMU body coordinate frame to the laser tracker frame. $\tilde{\boldsymbol{f}}_b$ represents noisy outputs from the tri-axial accelerometers. $\boldsymbol{\tau}_g$ and $\boldsymbol{\tau}_f$ are correlation times of the IMU dynamic bias errors. The diagonal matrix is expressed as $diag[\ ]$. The symbol $(\ )_\times$ represents anti-symmetric matrix. The system noise vector $\boldsymbol{\eta}$ complies with a Gaussian distribution $\boldsymbol{\eta} \sim N\{\boldsymbol{0}, \boldsymbol{Q}\}$, in which

$$\boldsymbol{Q} = diag \begin{bmatrix} \sigma_g^2 & \sigma_f^2 & \sigma_{g\delta b}^2 & \sigma_{f\delta b}^2 \end{bmatrix} \tag{4}$$

where $\boldsymbol{\sigma}_g$ and $\boldsymbol{\sigma}_f$ are respectively standard deviations of the gyroscopic and

accelerometers random noise errors, and $\sigma_{g\delta b}$ and $\sigma_{f\delta b}$ are the standard deviations of the dynamic bias errors. These specifications can be derived from real data by the Allan variance method or as specified in the IMU datasheet.

The IMU works in practice at discrete intervals of time. To cope with this, it is necessary to convert the model into a discrete form. The discrete error-state model can be expressed as

$$\delta\hat{x}_k = \boldsymbol{\Phi}_{k/k-1}\delta\hat{x}_{k-1} + \boldsymbol{G}_{k-1}\boldsymbol{\eta}_{k-1} \tag{5}$$

where $\delta\hat{x}_{k-1}$ and $\boldsymbol{\eta}_{k-1}$ are respectively the error state and system noise errors at time t_{k-1}. $\boldsymbol{\Phi}_{k/k-1}$ is the state transition matrix from time t_{k-1} to time t_k, and $\boldsymbol{G}_{k-1}$ is the appropriate error matrix. The matrix $\boldsymbol{\Phi}_{k/k-1}$ is derived by truncating the power-series expansion of the system matrix $\boldsymbol{F}$. The first-order solution is

$$\boldsymbol{\Phi}_{k/k-1} = \boldsymbol{I} + \boldsymbol{F}\tau_{imu} \tag{6}$$

3.1.2 Measurement Equations

The laser tracker provides the position and attitude signals for the 6D sensor unit, which are used as measurement updates for the Kalman filter. The differencing of the laser tracking measurements and the corresponding inertial system estimates introduces the measurement innovation. The measurement vector comprises the differences in attitude and position between the IMU and tracker:

$$\delta\hat{y} = \begin{bmatrix} \delta\hat{y}_\psi^T & \delta\hat{y}_p^T \end{bmatrix}^T = \begin{bmatrix} \hat{\psi}^T - \psi_{Tracker}^T & \hat{p}^T - p_{Tracker}^T \end{bmatrix}^T \tag{7}$$

where $\psi_{Tracker}$ and $p_{Tracker}$ are the sensor unit's Euler angles and 3D position measured by the laser tracker, $\hat{\psi}$ and $\hat{p}$ are corresponding derived values from the raw angular rates and accelerations, by a recursive dead reckoning process, and $\delta\hat{y}_\psi$ and $\delta\hat{y}_p$ are their differences.

The measurement model is given by

$$\delta\hat{y} = \boldsymbol{H}\delta\hat{x} + \boldsymbol{v} \tag{8}$$

where matrix $\boldsymbol{H}$ is known as the measurement matrix, and $\boldsymbol{v} \sim N\{\boldsymbol{0}, \boldsymbol{R}\}$ denotes the measurement error. The covariance matrix $\boldsymbol{R}$, is defined as

$$R = diag\begin{bmatrix} \sigma_\psi^2 & \sigma_p^2 \end{bmatrix} \tag{9}$$

whose diagonal entries σ_ψ^2 and σ_p^2 are respectively the variances of the measured Euler angles and 3D position, which are related to specific tasks. The critical parameter (Kalman gain) in this Kalman filter is dominated by the error noise covariance matrix rather than measurement noise covariance matrix. In general, the measurement noise covariance can be calculated according to the IMU manufacturer specifications, or by repetitive static measurements.

Since the laser tracker and IMU body frames are aligned, the measurement matrix consists simply of identity sub-matrices and null sub-matrices, expressed as

$$H = \begin{bmatrix} I & 0 & 0 & 0 & 0 & 0 & 0 \\ 0 & 0 & I & 0 & 0 & 0 & 0 \end{bmatrix} \tag{10}$$

3.1.3 Kalman Filter Algorithm

Equations (2) and (8) are the system and measurement equations that define the Kalman filter. At each arrival of a new laser tracking measurement, a measurement update is executed to generate the optimal estimates of the error states. Then the inertial system estimates at the measurement time are corrected. After this step, the IMU errors will continue to propagate, due to the random noise and uncompensated bias errors, until the next measurement comes. The equations for the Kalman filter are

$$
\begin{aligned}
\delta x_{k/k-1} &= \Phi_{k/k-1}\delta x_{k-1/k-1} \\
P_{k/k-1} &= \Phi_{k/k-1}P_{k-1/k-1}\Phi_{k/k-1}^T + Q_{k-1} \\
Q_{k-1} &= G_{k-1}Q\tau_{IMU}G_{k-1}^T \\
K_k &= \left(P_{k/k-1}H^T\right)\left(R + HP_{k/k-1}H^T\right)^{-1} \\
\delta x_{k/k} &= \delta x_{k/k-1} + K_k(\delta\hat{y}_k - H\delta x_{k/k-1}) \\
P_{k/k} &= (I - K_kH)P_{k/k-1}
\end{aligned} \tag{11}
$$

The first three equations comprise the system propagation (prediction) phase based on the previous best estimation, whilst the remaining steps comprise the measurement update (correction) phase. The subscript k is used to denote the IMU clock index. The time-propagated state estimates and covariance are denoted by $\delta x_{k/k-1}$ and $P_{k/k-1}$. Their counterparts following the measurement update are denoted by $\delta x_{k/k}$ and $P_{k/k}$. However, in the case of a laser tracker outage or during IMU cycles between successive tracker measurements, no measurement updates are available. Therefore, the measurement error covariance matrix norm will tend to ∞ and therefore the Kalman gain matrix K_k will be zero. The covariance matrix P should be set initially as a diagonal matrix before the first iteration, whose entries are chosen according to the expected variances of the initial error states.

After each measurement update, the inertial system estimates at the measurement time are corrected with the current best-estimate errors. Velocity and position can be

corrected by simply subtracting the estimated errors from the inertial system estimates of these quantities:

$$\hat{\boldsymbol{v}} = \tilde{\boldsymbol{v}} - \delta\hat{\boldsymbol{v}}$$
$$\hat{\boldsymbol{p}} = \tilde{\boldsymbol{p}} - \delta\hat{\boldsymbol{p}}$$
(12)

Attitude correction is applied by the direction cosine matrix representation:

$$\boldsymbol{R}\{\hat{\boldsymbol{\psi}}\} = (\mathbf{I} - [\delta\hat{\boldsymbol{\psi}}_{\times}])\boldsymbol{R}\{\tilde{\boldsymbol{\psi}}\}$$
(13)

where $\boldsymbol{R}\{\ \}$ is the rotation matrix associated to a set of decoupled Euler angles. The conversion between a rotation matrix and a set of Euler angles is described in [31].

3.2 Backward Smoothing Algorithm

In the previously described Kalman filter, no measurement update is made between tracker updates, which explicitly implies time-dependent error growth after a measurement update until the next measurement becomes available again. In continuous measurement, the estimation errors should be corrected at all IMU clock times. To reduce estimation errors during laser tracker measurement outages, backward smoothing is used. In this paper, a Rauch, Tung, and Striebel (RTS) method is applied [25], which is a very efficient fixed interval smoothing algorithm. The smoother the measurement information is, after as well as before the time of interest, the more precise the estimation is expected to be. In Fig.2 (b), the blue line is the integral process of IMU. Since the data of the 6D sensor occur at time $_{tracker(+)}$, the accumulated error eliminate suddenly. But the error during the t_{IMU} still exist. The backward smoothing algorithm starts with time $t_{tracker(+)}$ and reverses filtering fusion of data. The error is shown in the red line. Therefore, the backward smoothing algorithm is more accurate than the Kalman filter theoretically.

In the RTS method, a conventional Kalman filter runs forward in time as a first step. The error state vector $\delta\hat{\boldsymbol{x}}$, the error covariance matrix $\boldsymbol{P}$, after each system propagation and measurement update, and the transition matrix $\boldsymbol{\Phi}$, are recorded. Once the end of the data set is reached, smoothing begins, starting at the end and sweeping backwards. The smoothing gain on each iteration is given by:

$$\delta\boldsymbol{x}_{k/smooth} = \delta\boldsymbol{x}_{k/k} + \boldsymbol{A}_k(\delta\boldsymbol{x}_{k+1/smooth} - \delta\boldsymbol{x}_{k+1/k})$$
$$\boldsymbol{A}_k = \boldsymbol{P}_{k/k}\boldsymbol{\Phi}_{k+1/k}{}^T\boldsymbol{P}_{k+1/k}^{-1}$$
$$\boldsymbol{P}_{k/smooth} = \boldsymbol{P}_{k/k} + \boldsymbol{A}_k(\boldsymbol{P}_{k+1/smooth} - \boldsymbol{P}_{k+1/k})\boldsymbol{A}_k^T$$
(14)

where $\delta\boldsymbol{x}_{k/smooth}$ and $\boldsymbol{P}_{k/smooth}$ are the smoothed states and covariance matrix, respectively, $\delta\boldsymbol{x}_{k/k}$ and $\boldsymbol{P}_{k/k}$ are updated states and covariance matrix, respectively, and $\delta\boldsymbol{x}_{k+1/k}$ and $\boldsymbol{P}_{k+1/k}$ are predicted states and covariance matrix, respectively.

$\boldsymbol{A}_k$ is usually termed as a smoother gain matrix. Since the RTS smoother estimation is posteriori, its output will incur a lag. In practice, by making use of information from a limited period after the time of interest, the smoother can also be used to provide a quasi-real-time solution.

After the errors for all IMU clock times are estimated by the smoothing method, the inertial system estimates are corrected using Eqs. (12) and (13).

4. Experiments

A series of experiments were carried out to check the performance of the proposed method. A commercial 6D laser tracker (AT 901 LR & T-Mac, Leica Geosystems [26]) and a tactical-grade MEMS IMU (STIM 300, Sensonor AS [27]) were used for system integration. Figure 5(a) shows the experimental setup. The integrated 6D sensor unit is rigidly mounted on a turntable, approximately 100 mm from the rotation center. The laser tracker is placed about 4 m from the sensor. The spatial relationship between the 6D sensor and the IMU was calibrated prior to data collection. An expandable industrial PC was used to acquire, process and record data, as well as to control the sensors. The 6D laser tracker can provide a position accuracy of ± 15 μm + 6 μm/m and typical rotation accuracy of 0.01°. The functional specification of the IMU was measured beforehand using the Allan variance method, according to [32, 33], where data are collected for 20 hours after powering on for 2 hours, to achieve thermal stability. The attributes are listed in Table 1.
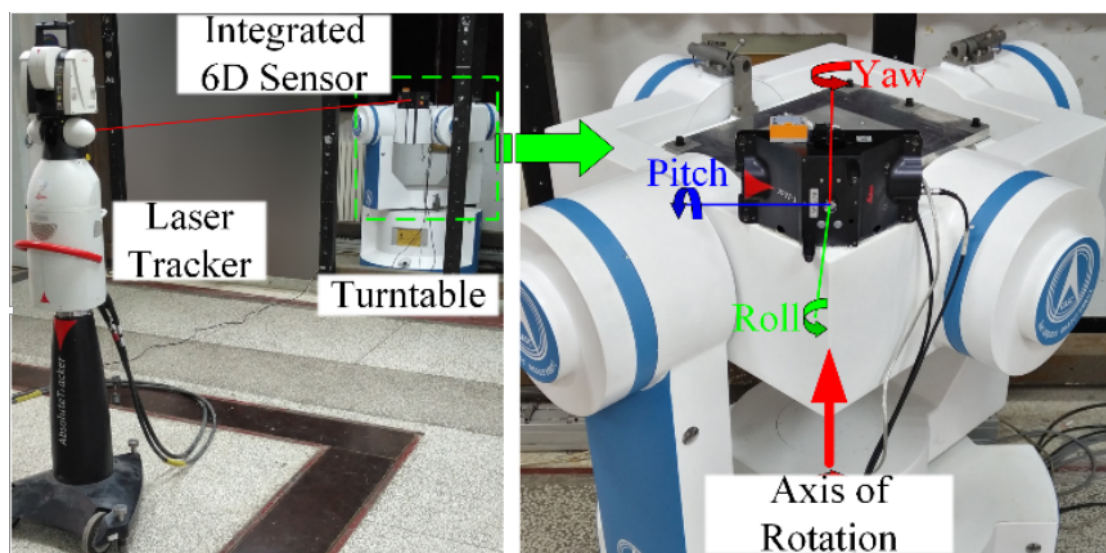
Figure 5. The experimental setup.

Table 1. Obtained specifications of STIM 300 from Allan variance analysis.

Parameter		X-Axis	Y-Axis	Z-Axis	Unit
Gyro					
Bias Instability		1.250	1.203	1.324	°/hr
Angular	Random	0.510	0.528	0.528	°/√hr

11

Walk				
Correlation Time	8000	8000	8000	s
Accelerometer				
Bias Instability	0.041	0.038	0.029	mg
Velocity Random Walk	0.132	0.138	0.108	m/s/√hr
Correlation Time	800	800	800	s

The turntable was programmed to rotate from -30° to 30° and was held stationary for a short period of time before and after rotation. Since the turntable can provide an angle accuracy of 1 arcsecond, the integrated sensor unit runs through a standard circular trajectory with a radius of the eccentric distance. The cubic spline interpolation of the angular and position trajectories of the 6D sensor unit at 100 Hz are used as references.

4.1 Different T-Mac frequencies

The purpose of these experiments is to observe the effect of different T-Mac frequencies on accuracy. The frequency of IMU was fixed to 2000 Hz and the rotating speed of turntable was 3 °/s. For performance comparison, the raw laser tracking data were set to 100 Hz, 50 Hz, 20 Hz, 10 Hz, 5 Hz, 2 Hz, and 1 Hz. Hence seven groups of datasets were fused using the proposed algorithm.

Fig. 6 shows fusion results at the measurement frequencies. To illustrate the actual behavior of the IMU accumulated error and make a comparison with our method, the results with Kalman filter only are also plotted. In Kalman curve, the trajectories become corrupt as the measuring laser tracker frequency decreases and the accumulated error drift dramatically until the next laser tracker measurement time comes. In comparison, the backward smoother is able to remove most of the accumulated errors of all IMU times. The drift effects are well-managed. The comparative experimental results illustrate that the backward smoothing procedure is essential for obtaining high fidelity results. It can also be seen that the gaps between adjacent laser tracking measurements are filled by the inertial system estimates. The data processing rate is increased from the laser tracker's measuring frequency to the IMU's sampling frequency. The angular measurements are also compared. They have similar performances.
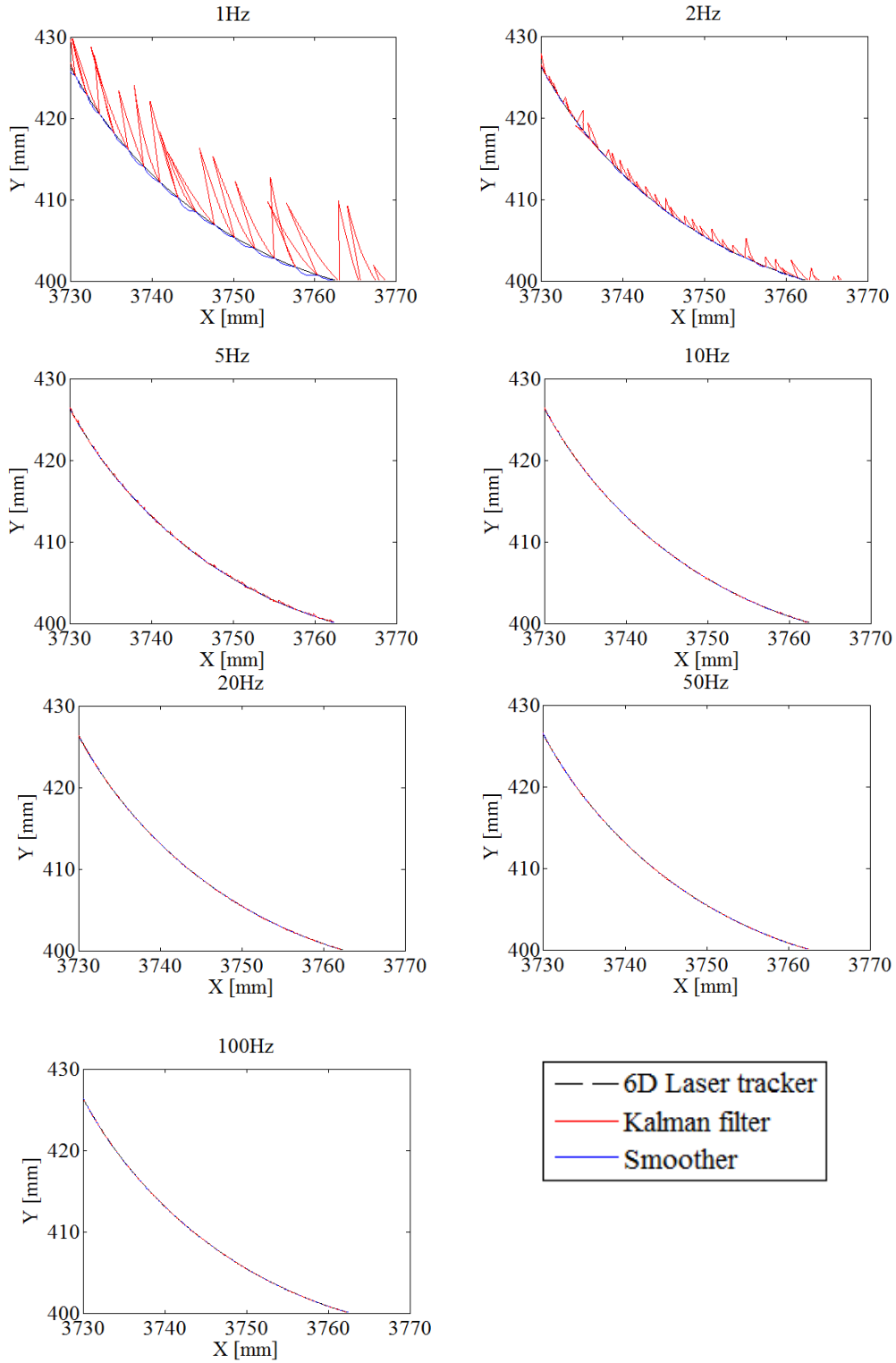
Figure 6. Estimated trajectories with different measuring frequencies, as well as 6D laser tracking trajectory. The blue lines are the backward smoothing results and the red lines are the results with Kalman filtering only, while the black dotted lines represent the laser tracking trajectories.

For each measuring frequency, the deviations of angle and position from each point to interpolated trajectory points were computed as errors. The statistical results of the deviations were evaluated. The root-mean-square (RMS) values are listed in Table 2.

In order to demonstrate the changes more clearly, the RMS values also show in Figure 7.

Table 2.   RMS Errors of different frequency

Frequency (Hz)	Approach	Roll (deg)	Pitch (deg)	Yaw (deg)	X (mm)	Y (mm)	Z (mm)
100	Kalman	0.0004	0.0006	0.0004	0.004	0.009	0.005
	Smoother	0.0001	0.0001	0.0001	0.003	0.005	0.003
50	Kalman	0.0008	0.0011	0.0008	0.005	0.010	0.006
	Smoother	0.0002	0.0002	0.0002	0.003	0.005	0.003
20	Kalman	0.0009	0.0013	0.0017	0.009	0.016	0.008
	Smoother	0.0002	0.0003	0.0003	0.003	0.005	0.003
10	Kalman	0.0012	0.0017	0.0028	0.025	0.038	0.017
	Smoother	0.0003	0.0004	0.0010	0.003	0.005	0.004
5	Kalman	0.0018	0.0024	0.0031	0.124	0.138	0.054
	Smoother	0.0005	0.0006	0.0018	0.008	0.009	0.008
2	Kalman	0.0029	0.0039	0.0066	1.182	1.318	0.376
	Smoother	0.0007	0.0009	0.0049	0.031	0.049	0.029
1	Kalman	0.0071	0.0075	0.0360	6.886	7.573	1.865
	Smoother	0.0015	0.0017	0.0326	0.106	0.259	0.130

Figure 7. The RMS trends of each angle and position change with different T-Mac frequencies. The blue and red lines show the RMS of the Kalman filter and Smoother results, respectively.

From Fig. 7, it can be inferred that the errors of both methods are close to zero when the measuring frequency is larger than 5 Hz. When the frequency of T-Mac is large enough, the two methods have little difference. However, if the frequency of T-Mac decreases, the proposed method shows better performance than the conventional Kalman filter alone.

4.2 Different rotating speeds

The purpose of these experiments is to observe the effect of different rotating speeds on accuracy. The frequency of IMU was set to 1000 Hz and only the RMS values of the proposed method are shown in Fig. 8. The frequencies of the T-Mac were set to 100 Hz, 50 Hz, 20 Hz, 10 Hz, 5 Hz, 2 Hz, and 1 Hz as in the previous experiments. The rotating speed of the turntable was set to 3°/s and 5°/s, respectively.

15
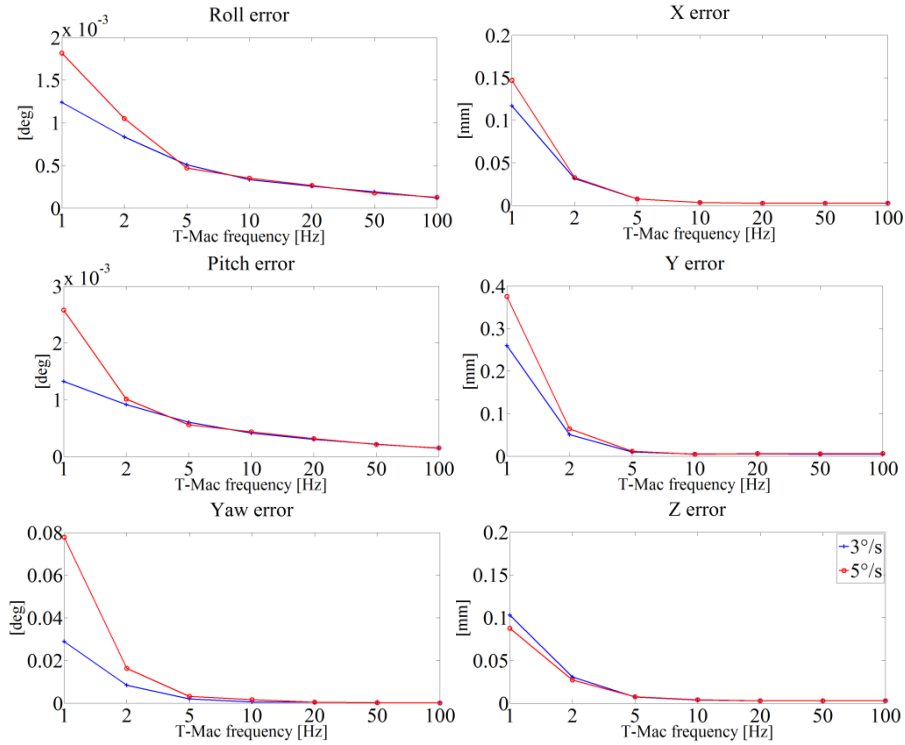
Figure 8. The RMS trends of each angle and position change with different T-Mac frequencies. When the rotating speed of turntable was 3°/s, the results are shown in red. When the speed was 5°/s, the results are shown in blue.

Figure 8 shows the RMS values of three positions and three rotational orientations at different rotating speeds of the turntable at different T-Mac frequencies. As shown in Figure 8, it can be inferred the rotating speed of turntable has no effect on measurement accuracy when the measuring frequency is larger than 5 Hz. However, as the frequency of T-Mac decreases, the RMS values increase significantly. The errors increase dramatically at the higher rotating speed. This indicates that lower movement speed is beneficial to improve accuracy during an outage.

4.3 Different IMU frequencies

The purpose of these experiments is to observe the effect of different IMU frequencies on accuracy. The frequency of the T-Mac was fixed to 2 Hz and the rotating speeding of the turntable was set to 3°/s. The frequency of the IMU was set to 500 Hz, 1000 Hz, and 2000 Hz, respectively. Both Kalman filter and Smoother results are shown in Fig. 9.
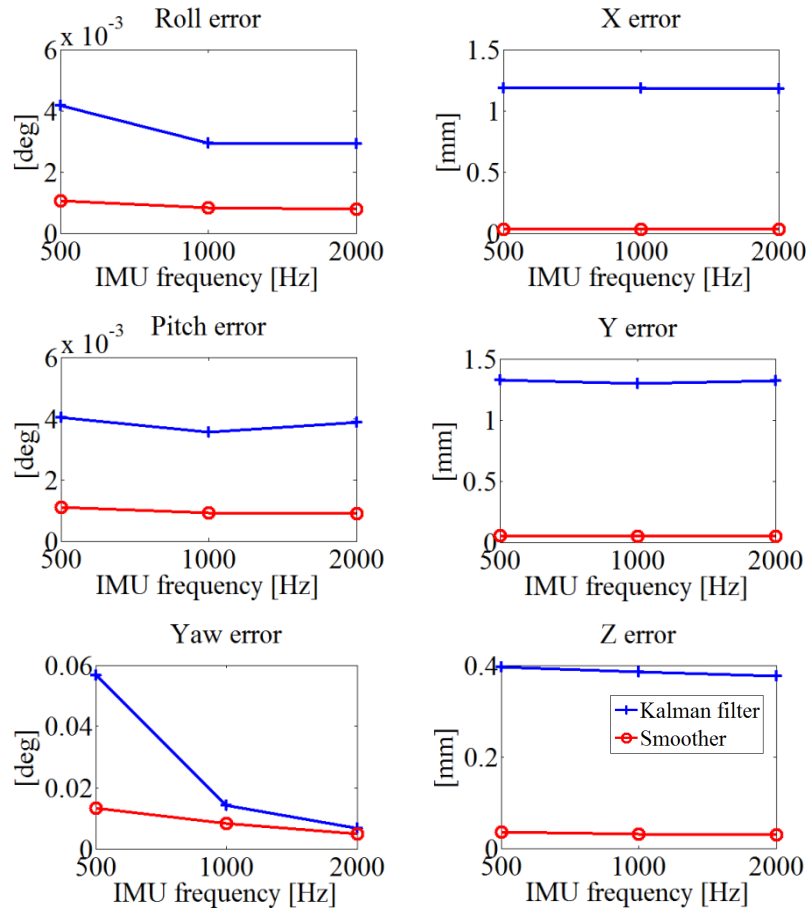
Figure 9. The RMS trends of each angle and position change with different IMU frequencies. The blue and red lines show the RMS of the Kalman filter only and Smoother, respectively.

From Fig.9, as the frequency of IMU increases, the errors of 6D in both Kalman filter and our smoother method are not regular. The reason is the frequency of IMU is high enough to make results irregular. It can be inferred that as the data rate is high enough, the frequency of IMU is not the main factor to affect data fusion accuracy.

4.4 Simulation

Besides real experiments, the simulations were designed to test the performance of the data fusion method in the outage case. The results involved fusing real IMU data at 2000 Hz and real laser tracker data at 20 Hz as references. The true values of the IMU and laser tracker data were generated from the references and downsampling to 500 Hz and 10 Hz, respectively. The simulated laser tracker data and IMU data were obtained by adding noise and bias errors to the reference values. For better graphical presentation, all trajectories were transformed into the IMU frame at the initial position. The simulation time is 90 seconds. For performance comparison, the outage durations of the laser tracker data occurred at 45 seconds and were set to 0.2, 0.5, 1, 2, 3, 5 seconds, respectively. Fig. 10 shows data fusion results with different outage periods. The error of the fitting trajectory of Kalman filter is clearly visible, especially when the outage duration is longer than 1 second. However, the data fusion results of backward

smoothing are convergent to the reference trajectory. Errors are also quantified as the differences between the data fusion results and the references during the outage period. The RMS values are listed in Table 3.
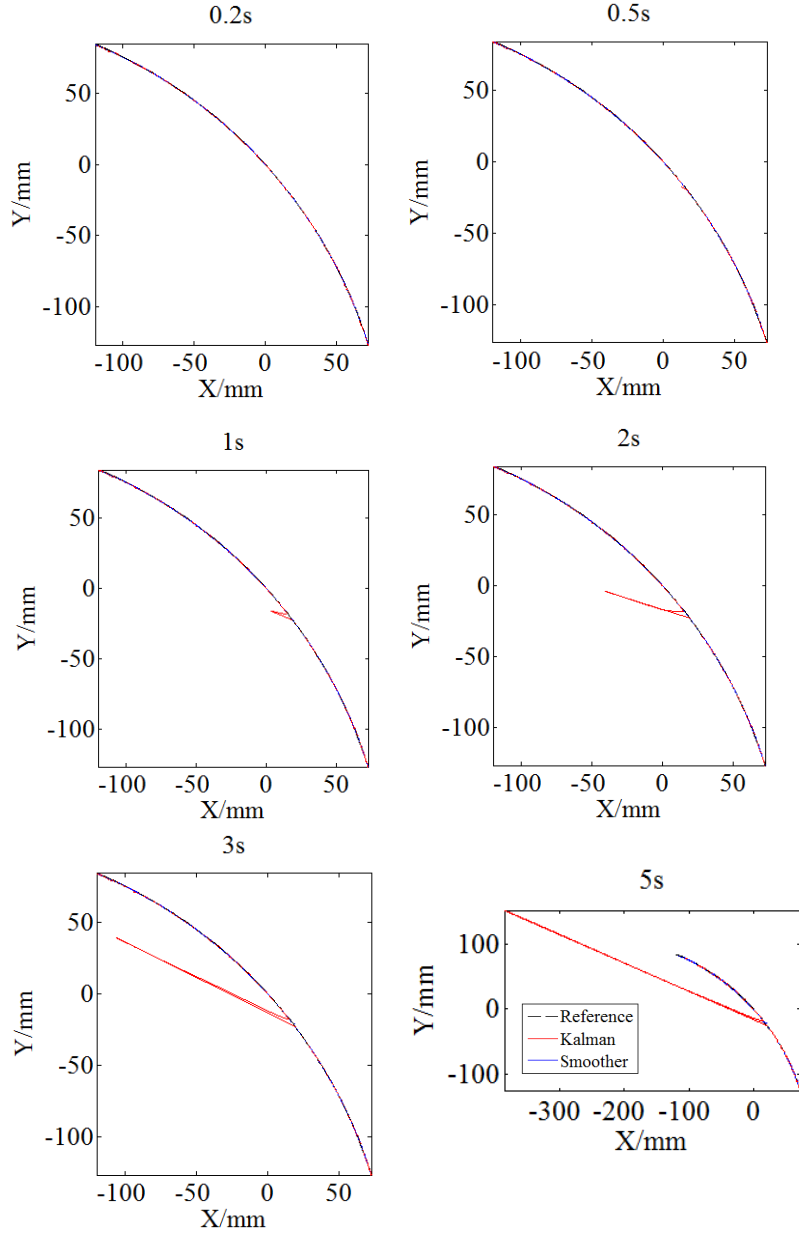
Figure 10 Estimated trajectories with different outage times, as well as the reference trajectory. The blue solid lines are the backward smoothing results and the red solid lines are the results with Kalman filter only, while the black dotted lines represent the simulation reference.

Table 3. RMS Errors of different interruption time

Interruption Time (s)	Approach	Roll (deg)	Pitch (deg)	Yaw (deg)	X (mm)	Y (mm)	Z (mm)
0.2	Kalman	0.0020	0.0035	0.0040	0.205	0.117	0.001

	Smoother	0.0035	0.0052	0.0015	0.029	0.020	0.017
0.5	Kalman	0.0021	0.0053	0.0030	1.261	0.662	0.095
	Smoother	0.0030	0.0043	0.0011	0.070	0.035	0.031
1	Kalman	0.0072	0.0122	0.0020	6.582	3.628	0.509
	Smoother	0.0031	0.0044	0.0009	0.102	0.038	0.015
2	Kalman	0.0073	0.0106	0.0015	23.090	7.824	1.076
	Smoother	0.0067	0.0126	0.0008	0.106	0.127	0.155
3	Kalman	0.0066	0.0151	0.0014	50.760	22.890	3.514
	Smoother	0.0049	0.0144	0.0008	0.325	0.261	0.423
5	Kalman	0.0126	0.0344	0.0013	126.400	73.570	6.057
	Smoother	0.0082	0.0125	0.0007	1.369	1.932	0.668

As shown in Table 3, outage periods affect the accuracy of the 6D measurement results. With the Kalman filter only, when the information provided by the laser tracker is interrupted over 0.5 seconds, the error of position is greater than 1 mm. However, using the backward smoothing algorithm, when the interruption time is less than 3 seconds, the position error is still less than 0.5 mm. The similar improvements can also be seen in the angle measurements. Therefore, for outages of 2 to 3 seconds, the integrated system can yield high fidelity 6D measurements results.

5. Conclusions

In this paper, a backward smoothing algorithm combined with a Kalman filter is proposed to enhance 6D Measurement by integrating an IMU with a 6D sensor unit (T-Mac) of a laser tracker. The distinct advantage of the proposed method is that the data acquisition rates of the integrated system are increased from the laser tracker's inherent measuring frequency to the IMU's sampling frequency. Hence, it is able to estimate the 6D measurements during an outage period of a laser tracker. According to analysis and evaluation, the following conclusions can be drawn:

(a) The proposed data fusion method is more stable than using a classical Kalman filter only, especially when the acquisition frequency of the 6D sensor unit of the laser tracker is reduced.

(b) The movement speed of the integrated system is related to accuracy. During an outage or period of low-frequency operation of the T-Mac, low speed performs high precision. Furthermore, the frequency of the IMU is high enough that it does not affect measurement accuracy in practical applications.

(c) The proposed fusion method corrects most of the IMU errors at the end of the outage intervals. According to the experiments and simulations, the proposed algorithm is valid when the laser tracker frequency is down to 1 Hz. It also supports an outage period of the laser tracker within 3 seconds.

Therefore, the method in this paper expands the application scope for a 6D sensor unit of a laser tracker. It is possible to increase measurement speed and mitigate the effect of line of sight blockages during measurements for a short period.

Acknowledgments

References

[1] S. Shi, Z. Wang, K. Zhao, Z. You, C. Ouyang, "MFVS/MIMU integrated 6-DOF autonomous navigation in known environments with extremely simple landmarks," Aerosp. Sci. Technol., 2018, 75, 329-341.

[2] Y. Liu, R. Xiong, Y. Wang, H. Huang, X. Xie, X. Liu, G. Zhang, "Stereo Visual-Inertial Odometry with Multiple Kalman Filters Ensemble," IEEE T. Ind. Electron., 2016, 63(10), 6205-6216.

[3] Y. S. Suh, "A smoother for attitude and position estimation using inertial sensors with zero velocity intervals," IEEE Sens. J., 2012, 12(5), 1255-1262.

[4] Y. S. Suh, "Inertial sensor-based smoother for gait analysis," Sensors, 2014, 14(12), 24338-57.

[5] C. N. K. Nam, H. J. Kang, Y. S. Suh, "Golf swing motion tracking using inertial sensors and a stereo camera," IEEE T. Instrum. Meas., 2014, 63(4), 943-952.

[6] S. M. Ayaz, K. Danish, J. Y. Bang, S. I. Park, Y. Roh, M. Y. Kim, "A multi-view stereo based 3D hand-held scanning system using visual-inertial navigation and structured light," MATEC Web of Conferences, 2015, 32, 06004.

[7] B. Sun, J. Zhu, L. Yang, S. Yang, Y. Guo, "Sensor for in-motion continuous 3D shape measurement based on dual line-scan cameras," Sensors 2016, 16(11), 1949.

[8] B. Muralikrishnan, S. Phillips, and D. Sawyer, "Laser trackers for largescale dimensional metrology: A review," Precis. Eng., 2016, 44, 13-28.

[9] R. H. Schmitt, M. Peterek, E. Morse, W. Knapp, M. Galetto, F. Hartig, G. Goch, B. Hughes, A. Forbes, W. T. Estler , "Advances in large-scale metrology – review and future trends," CIRP Ann. – Manuf. Techn.,2016, 65(2), 643-665.

[10] S. Kyle, "Alternatives in 6DOF probing - more flexibility, lower cost, universal," in the

Proceedings of the 21st Annual Coordinate Metrology Systems Conference, 2005.

[11] K. Lau, Y. Yang, Y. Liu, and H. Song, "Dynamic performance evaluation of 6D laser tracker sensor," in the Proceedings of the 10th Performance Metrics for Intelligent Systems Workshop, 2010.

[12] J. A. Gordon, D. R. Novotny, A. E. Curtin, "A single pixel touchless laser tracker probe," Journal of the CMSC, 2015, 10(2), 12-21.

[13] S. Kyle, "Optically jointed probing systems for large volume coordinate metrology," in the Coordinate Measurement Systems Conference (CMSC), 2006.

[14] S. Kyle, "Roll angle in 6DOF tracking," in the Coordinate Measurement Systems Conference (CMSC), 2008.

[15] R. E. Bridges, D. H. Parker, "Six-degree-of-freedom laser tracker that cooperates with a remote projector to convey information," U.S. Patent, 2014, no. 8848203.

[16] J. Lin, K. Gao, Z. Wang, "Combined measurement system for double shield tunnel boring machine guidance based on optical and visual methods, " J. Opt. Soc. Am. A, 2017, 34(10):1810-1816.

[17] R. N. Dean Jr, A. Luque, "Applications of microelectromechanical systems in industrial processes and services," IEEE T. Ind. Electron., 2009, 56(4), 913-925.

[18] F. Aghili, A. Salerno, "Driftless 3-D attitude determination and positioning of mobile robots by integration of IMU with two RTK GPSs," IEEE/ASME T. Mech., 2013, 18(1), 21-31.

[19] F. M. Mirzaei, S. I. Roumeliotis, "A Kalman filter-based algorithm for IMU-camera calibration: observability analysis and performance evaluation," IEEE T. Robot., 2008, 24(5), 1143-1156.

[20] T. Lupton, S. Sukkarieh, "Visual-inertial-aided navigation for high-dynamic motion in built environments without initial conditions," IEEE T. Robot., 2012, 28(1), 61-76.

[21] S. H. P. Won, W. W. Melek, F. Golnaraghi, 2010, "A Kalman/particle filter-based position and orientation estimation method using a position sensor/inertial measurement unit hybrid system," IEEE T. Ind. Electron., 2010, 57(5), 1787-1798.

[22] S. Y. Chen, "Kalman filter for robot vision: a survey," IEEE T. Ind. Electron., 2012, 59(11), 4409-4420.

[23] F. Auger, M. Hilairet, J. M. Guerrero, E. Monmasson, T. Orlowska-Kowalska, S. Katsura, "Industrial applications of the Kalman filter: a review," IEEE T. Ind. Electron., 2013, 60(12), 5458-5471.

[24] X. Gao, T. Zhang, Y. Liu, Q. R. Yan, "Visual SLAM XIV: From Theory to Practice," Beijing: Publishing House of Electronics Industry, 2017.

[25] R. G. Brown, P. Y. C. Hwang. "Introduction to random signals and applied Kalman filtering with Matlab exercises," 4th Edition. New York: Wiley, 2012.

[26] Leica Geosystems. Available online: http://www.leicageosystems.us/en/Leica-T-Mac_66262.htm (accessed on Feb. 2017).

[27] Sensonor AS. Available online: http://www.sensonor.com/gyroproducts/inertial-measurement-units/stim300.aspx (accessed on Feb.2017).

[28] B. Liu, J. Fang, "Modified hybrid calibration method for IMU without orientation", Chinese Journal of Scientific Instrument, 2008, 28(6), 1250-1254.

[29] R. Gonzalez, J. I. Giribet, H. D. Patino, "An approach to benchmarking of loosely coupled

low-cost navigation systems," Mathematical and Computer Modelling of Dynamical Systems, 2015, 21(3), 272-287.

[30] P. D. Groves, Principles of GNSS, inertial, and multisensor integrated navigation systems, 3rd Ed., Boston, USA: Artech house, Ch. 14, p. 577-582, 2013.

[31] Z. Y. Zhang, "A flexible new technique for camera calibration," IEEE Trans. Pattern Anal. Mach. Intell. 2000, 22(11), 1330-1334.

[32] "IEEE Standard Specification Format Guide and Test Procedure for Single-Axis Interferometric Fiber Optic Gyros," IEEE Std., 952-1997, 1998.

[33] N. Ei-Sheimy, H. Hou, X. Niu, "Analysis and modeling of inertial sensors using Allan variance," IEEE T. Instrum. Meas., 2008, 57(1), 140-149.

Zoom camera

Laser Tracker

Line of sight of LED Markers

IMU

Line of sight of retro-reflector

6D Sensor

Retro-reflector

LED Markers

Gaps between Successive Measurements

$t_{tracker}(-)$ $t_{tracker}$ Beginning of Outage $t_{tracker}(+)$

Laser Tracker   Loss of Line of Sight

Errors

Kalman

Back Smoother

Accumulated Error

End of outage

$t_{tracker}$ t_{IMU} ··· $t_{tracker}(+)$

(a)   (b)

Angular Rates and Accelerations $\tilde{\boldsymbol{\omega}}_b$ $\tilde{\boldsymbol{f}}_b$ → Bias corrections $\hat{\boldsymbol{\omega}}_b$ $\hat{\boldsymbol{f}}_b$ → Attitude Update Velocity Update Position Update $\tilde{\boldsymbol{\psi}}$ $\tilde{\boldsymbol{v}}$ $\tilde{\boldsymbol{p}}$ → $\otimes$ → $\hat{\boldsymbol{\psi}}$ $\hat{\boldsymbol{v}}$ $\hat{\boldsymbol{p}}$

$\hat{\boldsymbol{b}}_g$ $\delta\hat{\boldsymbol{b}}_g$ $\hat{\boldsymbol{b}}_f$ $\delta\hat{\boldsymbol{b}}_f$

Kalman Filter $\delta\hat{\boldsymbol{\psi}}$ $\delta\hat{\boldsymbol{v}}$ $\delta\hat{\boldsymbol{p}}$

$\boldsymbol{\psi}_{Tracker}, \boldsymbol{p}_{Tracker}$

Tracker Measurements

STIM300

Synchronizing

Calibration

Roll error, X error, Pitch error, Y error, Yaw error, Z error — Kalman filter, Smoother — as a function of T-Mac frequency [Hz].

Roll error

X error

Pitch error

Y error

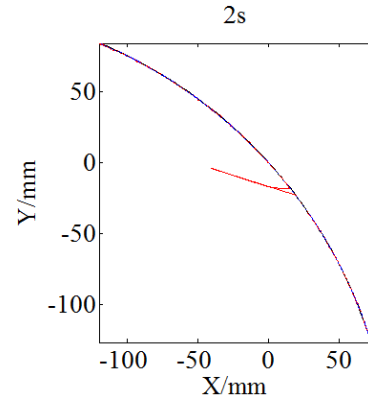Yaw error
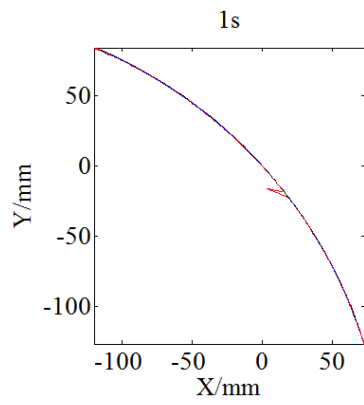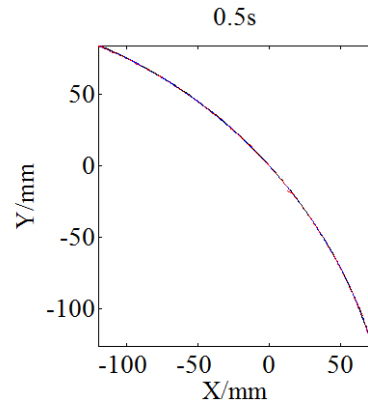
Z error

[deg]

[mm]

T-Mac frequency [Hz]

3°/s
5°/s

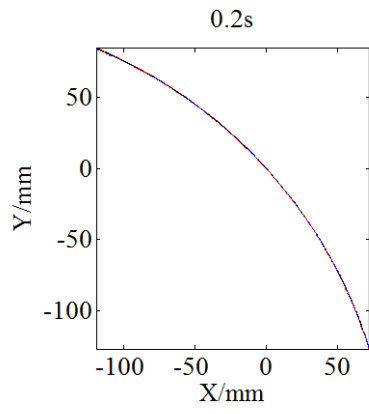**Table 1. Obtained specifications of STIM 300 from Allan variance analysis.**

Parameter	X-Axis	Y-Axis	Z-Axis	Unit
Gyro				
Bias Instability	1.250	1.203	1.324	°/hr
Angular Random Walk	0.510	0.528	0.528	°/√hr
Correlation Time	8000	8000	8000	s
Accelerometer				
Bias Instability	0.041	0.038	0.029	mg
Velocity Random Walk	0.132	0.138	0.108	m/s/√hr
Correlation Time	800	800	800	s

Table 2.   RMS Errors of different frequency

Frequency (Hz)	Approach	Roll (deg)	Pitch (deg)	Yaw (deg)	X (mm)	Y (mm)	Z (mm)
100	Kalman	0.0004	0.0006	0.0004	0.004	0.009	0.005
	Smoother	0.0001	0.0001	0.0001	0.003	0.005	0.003
50	Kalman	0.0008	0.0011	0.0008	0.005	0.010	0.006
	Smoother	0.0002	0.0002	0.0002	0.003	0.005	0.003
20	Kalman	0.0009	0.0013	0.0017	0.009	0.016	0.008
	Smoother	0.0002	0.0003	0.0003	0.003	0.005	0.003
10	Kalman	0.0012	0.0017	0.0028	0.025	0.038	0.017
	Smoother	0.0003	0.0004	0.0010	0.003	0.005	0.004
5	Kalman	0.0018	0.0024	0.0031	0.124	0.138	0.054
	Smoother	0.0005	0.0006	0.0018	0.008	0.009	0.008
2	Kalman	0.0029	0.0039	0.0066	1.182	1.318	0.376
	Smoother	0.0007	0.0009	0.0049	0.031	0.049	0.029
1	Kalman	0.0071	0.0075	0.0360	6.886	7.573	1.865
	Smoother	0.0015	0.0017	0.0326	0.106	0.259	0.130

Table 3.   RMS Errors of different interruption time

Interruption Time (s)	Approach	Roll (deg)	Pitch (deg)	Yaw (deg)	X (mm)	Y (mm)	Z (mm)
0.2	Kalman	0.0020	0.0035	0.0040	0.205	0.117	0.001
	Smoother	0.0035	0.0052	0.0015	0.029	0.020	0.017
0.5	Kalman	0.0021	0.0053	0.0030	1.261	0.662	0.095
	Smoother	0.0030	0.0043	0.0011	0.070	0.035	0.031
1	Kalman	0.0072	0.0122	0.0020	6.582	3.628	0.509
	Smoother	0.0031	0.0044	0.0009	0.102	0.038	0.015
2	Kalman	0.0073	0.0106	0.0015	23.090	7.824	1.076
	Smoother	0.0067	0.0126	0.0008	0.106	0.127	0.155
3	Kalman	0.0066	0.0151	0.0014	50.760	22.890	3.514
	Smoother	0.0049	0.0144	0.0008	0.325	0.261	0.423
5	Kalman	0.0126	0.0344	0.0013	126.400	73.570	6.057
	Smoother	0.0082	0.0125	0.0007	1.369	1.932	0.668

Conflict of interest statement

We declare that we do not have any commercial or associative interest that represents a conflict of interest in connection with the work submitted.